Electronic Supplementary Information (ESI)

Laser-assisted High-performance PtRu Alloy for pH-Universal Hydrogen Evolution

Beibei Pang,[a] Xiaokang Liu,[a] Tianyang Liu,[c] Tao Chen,[a,d] Xinyi Shen,[a] Wei Zhang,[a] Sicong Wang,[a] Tong Liu,[a] Dong Liu,[a] Tao Ding,[a] Zhaoliang Liao,[a] Yafei Li,[c] Changhao Liang,[b]* Tao Yao[a]**

[a]National Synchrotron Radiation Laboratory, University of Science and Technology of China, Hefei 230029, P.R. China.

[b]Key Laboratory of Materials Physics and Anhui Key Laboratory of Nanomaterials and Nanotechnology, Institute of Solid State Physics, Hefei Institutes of Physical Science, Chinese Academy of Sciences, Hefei 230031, China.

[c]Jiangsu Collaborative Innovation Centre of Biomedical Functional Materials, Jiangsu Key Laboratory of New Power Batteries, School of Chemistry and Materials Science, Nanjing Normal University, Nanjing 210023, China.

[d]School of National Defense Science and Technology, Southwest University of Science and Technology, Mianyang, 621010, China.

Corresponding authors: liyafei@njnu.edu.cn (Yafei Li); chliang@issp.ac.cn (Changhao Liang); yaot@ustc.edu.cn (Tao Yao)

Materials and Methods

Materials. All chemicals were of analytical grade and used without further purification. Chloroplatinic acid hexahydrate ($H_2PtCl_6 \cdot 6H_2O$), ruthenium chloride ($RuCl_3$), concentrated nitric acid (HNO_3, 65 wt.%), and ethanol are purchased from Sinopharm Chemical Reagent Co., Ltd. (China). Commercial 20 wt.% Pt/C (JM Pt/C, Hispec 3000) was purchased from Shanghai Hesen Electric Co., Ltd. Graphite powder (XF011 7782-42-5) and carbon nanotubes (XFM13 1333-86-4) were obtained from XFNano Materials Tech Co., Ltd.

Synthesis of mCNTs. 600 mg of carbon nanotubes were first refluxed in 100 mL of HNO_3 solution at 120 °C for 6 h. Surface-modified carbon nanotubes remarked as mCNTs were washed thoroughly with deionized water, then dried at 60 °C for further use.

Synthesis of M/mCNTs (M= Pt, Ru or PtRu). Firstly, 5 mg of m-CNTs, 2 μmol of $H_2PtCl_6 \cdot 6H_2O$, and 8 μmol $RuCl_3$ were dispersed in 15 ml ethanol solution. Then the mixture was irradiated by Nd: YAG laser with parameters of 355 nm wavelength, 10 mJ pulse energy, 20 Hz frequency, 6 mm beam size, and 7 ns pulse duration for 60 min. The resultant product was washed several times with deionized water and ethanol through centrifugation at 10,000 rpm. Finally, the product was dried at 60 °C for further characterization and electrochemical tests. As controls, Ru/mCNTs and Pt/mCNTs monometallic catalysts were synthesized following the same procedure with only $RuCl_3$ or $H_2PtCl_6 \cdot 6H_2O$ used in the LIL process.

Material characterizations. The crystalline structures were determined through X-ray diffractometer (XRD) by using a Philips X' Pert system with Cu Kα (λ = 1.54 Å). The high-resolution transmission electron microscopy (HRTEM) images and high-angle annular dark-field scanning transmission electron microscopy (HAADF-STEM) were carried out on a transmission electron microscopy (TEM, (JEOL, JEM-2010)) with 200 kV acceleration voltages, which was equipped with an Oxford INCA energy-dispersive X-ray spectroscope for microscopic elemental analysis. Raman spectroscopy analysis was carried on a UV-visible-near-infrared spectrometer (Cary-5E) with a laser wavelength of 532 nm. The chemical valence and surface elements of the electrocatalysts were detected using X-ray photoelectron spectroscopy (XPS) on a Thermo ESCALAB250Xi spectrometer with an excitation source of monochromatized Al Kα (hv = 1486.6 eV) and a pass energy of 30 eV. The mass of metal content within the mCNTs nanocomposites was determined through inductively coupled plasma atomic emission spectrometry (ICP-AES), all samples were weighed and digested in aqua regia for 24 h.

Electrochemical Measurements. All of the electrochemical measurements were performed in a typical three-electrode system on an electrochemical workstation (CHI760E, Chen Hua, Shanghai, China). A blank carbon paper and Ag/AgCl (3 M KCl solution) electrodes were used as the counter electrode and the reference electrode, respectively. All composites catalysts were drop-cast on a glassy carbon electrode with a diameter of 3 mm (0.07065 cm^2), the coated glassy carbon was used as the working electrode. The glassy carbon electrode was polished on a microfiber polishing cloth with a small volume of 0.3 μm alpha alumina powder until the mirror finish before all experiments. To prepare the catalyst ink, 5 mg catalyst was mixed with 750 μL deionized water, 250 μL ethanol, and 100 μL Nafion (0.5 wt%) by sonicating for 1 h to form a homogeneous ink. Then 6.0 μL of the catalyst ink (containing 0.0273 mg of catalyst) was loaded onto the glassy carbon electrode (loading 0.386 mg cm^{-2}). Finally, the as-prepared catalyst film was dried at room temperature. Linear sweep voltammetry (LSV) with a scan rate of 5 mV s^{-1} was conducted in N_2-saturated 1 M KOH, 0.5 M H_2SO_4, or 1 M PBS. The electrochemical durability was conducted by 3,000 cyclic voltammetry sweeps (CV) between 0∽-0.2 V (vs. RHE), 0.2∽-0.1 V (vs. RHE), and 0∽-0.3 V (vs. RHE) at 0.1 V s^{-1} in 1 M KOH, 0.5 M H_2SO_4 and 1 M PBS solution, respectively. The durability of the PtRu/mCNTs was also investigated through chronopotentiometry (CP) tests, and the timed-pendent voltage was recorded under a static current density of 10 mA cm^{-2} for 48 h. All polarization curves were 80% iR-corrected and all potentials were reference to the RHE.

Operando XAFS measurements. Samples of 20 mg were homogeneously mixed with 40 mg graphite and hence pressed into circular pellets with a diameter of 8 mm for further X-ray absorption fine structure (XAFS) measurement under ambient conditions. The Pt L_3-edge (11564 eV) and Ru K-edge (22117 eV) XAFS spectra were performed at the BL14W1 beamline of the Shanghai Synchrotron Radiation Facility (SSRF), China. During XAFS measurements, we calibrated the position of the absorption edge (E_0) using Pt foil and Ru foil, respectively. And all the XAFS data were collected during one period of beam time. Each spectrum was measured three times to ensure the repeatability of the data (the positions of E_0 were almost the same during the multiple scans). The position of E_0 is defined as the point corresponding to the maximum value in the derivative curves of the XANES spectra.

XAFS data analysis. Acquired EXAFS data were processed according to standard procedures using the ATHENA module implemented in the IFEFFIT software packages. The Pt L_3-edge and Ru K-edge k^2-weighted χ(k) data in the k-space ranging from 2.3 to 10.4 $Å^{-1}$ and 2.9 to 12.5 $Å^{-1}$ were Fourier-transformed to real (R) space using a Hanning windows (dk=1.0 $Å^{-1}$) to

separate the EXAFS contributions from different coordination shells. To obtain the detailed structural parameters around the Pt and Ru atoms in PtRu alloy, quantitative curve fittings were carried out for the Fourier-transformed $k^2\chi(k)$ in R-space using the ARTEMIS module of IFEFFIT. Effective backscattering amplitudes F(k) and phase shifts Φ(k) of all fitting paths were calculated with the ab initio code FEFF8.054. For PtRu alloy, the k-range of 2.3-10.4 $Å^{-1}$ and 2.9 to 12.5 $Å^{-1}$ at Pt L_3-edge and Ru K-edge respectively were used and curve fittings were carried out in R-space within a R range of [1.0, 3.2] Å for k^2-weighted χ(k) functions. The number of independent points:

$$N_{ipt} = 2\Delta k \times \Delta R/\pi = 2 \times (10.4-2.3) \times (3.2-1.0)/\pi = 11 \qquad \text{(Pt } L_3\text{-edge)}$$

$$N_{ipt} = 2\Delta k \times \Delta R/\pi = 2 \times (12.5-2.9) \times (3.2-1.0)/\pi = 13 \qquad \text{(Ru K-edge)}$$

For Pt L_3-edge of ex situ PtRu alloy sample, the FT curve showed two peaks at 1.87 Å and 2.47 Å assigned to the Pt-Cl and Pt-Ru coordination. Subsequently, a two-shell structure model including Pt-Cl and Pt-Ru scattering paths were used to fit the EXAFS data of the operando samples. For Ru K-edge, the FT curve showed a peak at 1.50 Å assigned to the Ru-O coordination and 2.36 Å assigned to the Ru-Metal coordination. Subsequently, a three-shell structure model including one Ru-O and two Ru-M scattering paths were used to fit the EXAFS data of the operando samples, where the Ru-Pt path denotes the Pt atoms at the surface of Ru NPs.

During curve fittings, the amplitude reduction factor S_0 was fixed at the value of 0.81 for Pt samples determined by fitting the data of Pt foil, with the coordination number of Pt-Pt set as 12 according to the face-centred cubic (fcc) structure. For the Pt-Cl and Pt-Ru paths of EXAFS samples at Pt-L_3 edge, including the ex situ sample, the open circuit sample and the samples under electrochamical reaction, the Debye-Waller factors (σ^2) coordination numbers (CN), interatomic distances (R) and energy shift (ΔE_0) are set as free parameters. Therefore, the number of adjustable parameters is

$$N_{para} = 4 + 4 = 8 < N_{ipt} = 11 \qquad \text{(Pt } L_3\text{-edge)}$$

For the fittings of EXAFS data at Ru K-edge, the S_0^2 of all samples were set as 0.80 according to the fitting of Ru foil. During the fittings for Ru K-edge, we constructed a three-shell structure model, including Ru-O path, Ru-Ru path and Ru-Pt path. For the sample in air, all parameters were set adjustable, so that the number of adjustable parameters is $N_{para}=4 + 4 + 4 = 12 < N_{ipt} = 13$. Considering the major component of nanoparticles are Ru, in the rest fittings for the operando samples, the CN of Ru-Pt path were set equal to that of in air sample, which is 8.5, while all other parameters were treated as adjustable parameters. The number of adjustable parameters is

$N_{para} = 4 + 4 + 2 + 2 = 12 < N_{ipt} = 13$ (Ru K-edge)

All yielded R factors of Pt L_3-edge and Ru K-edge fittings are not larger than 0.020, indicating the appropriate modeling, rational parameter settings and thus, the good fitting qualities.

Computational methods. Density functional theory (DFT) computations were performed using plane-wave basis set in the Vienna ab initio Simulation Package (VASP)[1]. The ion-electron interaction was described with the projector-augmented-wave (PAW) method[2, 3]. The exchange-correlation energy term was expressed by Perdew-Burke-Ernzerhof (PBE) functional and based on the generalized gradient approximation (GGA)[4]. Cut-off energy was set to 460 eV. The total energy and force convergence was set as 5×10^{-5} eV and -0.05 eV/Å, respectively. And the Brillouin zone was represented by the Monkhorst-Pack special k-point mesh of 3×3×1 or 7×7×1 for geometry optimization and electronic structure computations. DFT-D3 (D stands for dispersion) procedure was adopted to describe the van der Waals (vdW) interactions[5]. To calculate accurately, the solvation effect was also considered with the Poisson-Boltzmann implicit solvation model, and the dielectric constant of water was set as 80[6].

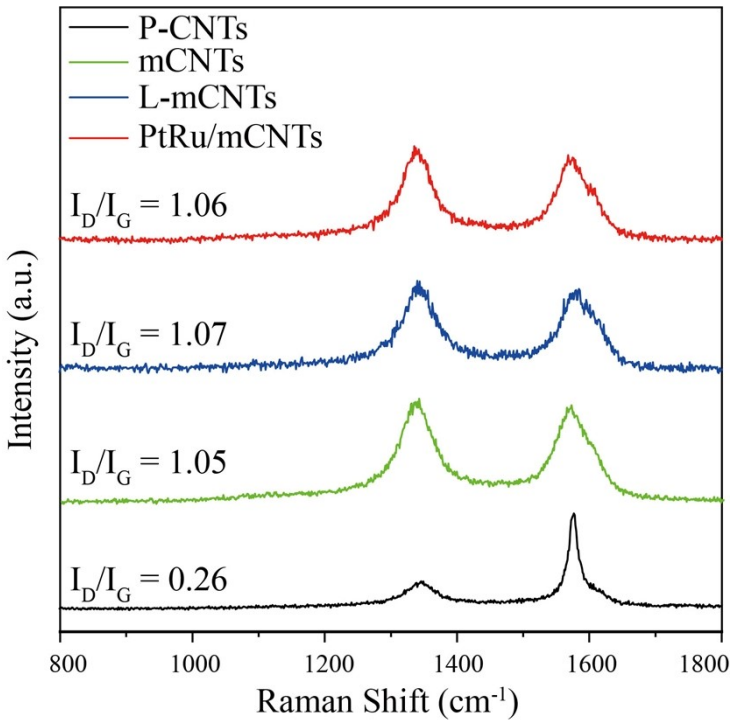

Fig. S1. Typical Raman spectra of CNTs before and after 355 nm laser irradiation.

All samples show a D-band at 1350 cm^{-1} representing the edge planes and disordered structures, and the characteristic G-band at 1580 cm^{-1} ascribed to the ordered sp^2 bonded carbon. The I_D/I_G values of mCNTs were significantly increased compared with P-CNTs shown in this figure, confirming the successful introduction of oxygen-containing functional group. Simultaneously, compared with harsh acid oxidation treatment, laser irradiated mCNTs (L-CNTs) did not cause further damage to the structure of mCNTs, which ensured that the conductivity of mCNTs was not weakened.

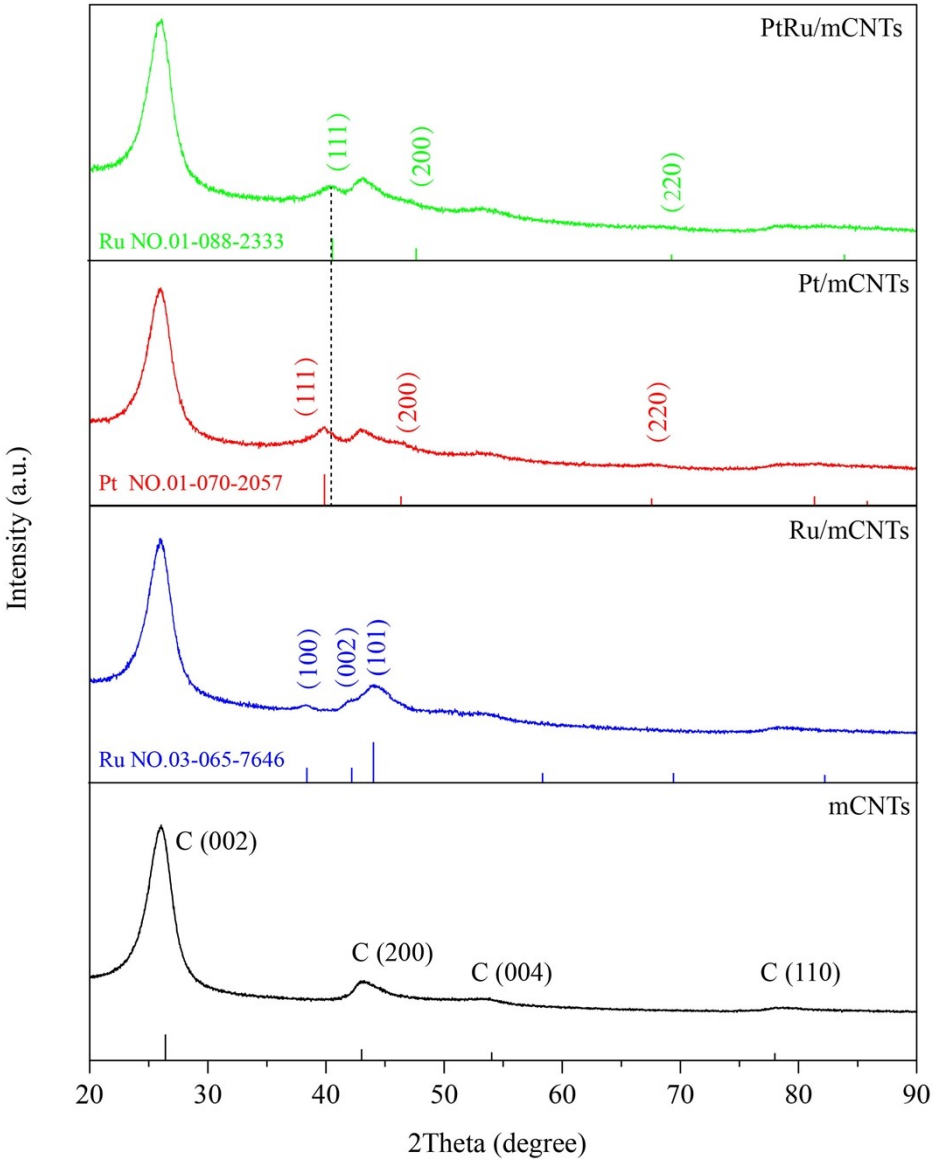

Fig. S2. XRD patterns of PtRu/mCNTs, Pt/mCNTs, Ru/mCNTs, and mCNTs.

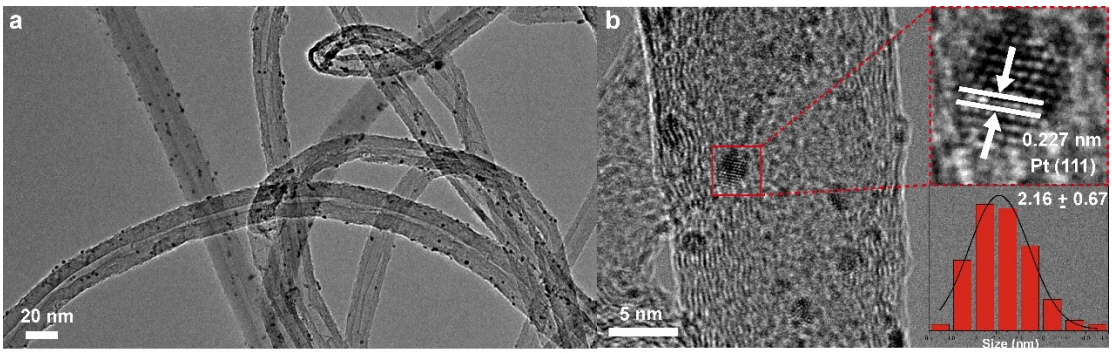

Fig. S3. The low-magnification TEM (a) and (b) HRTEM image of Pt/mCNTs.

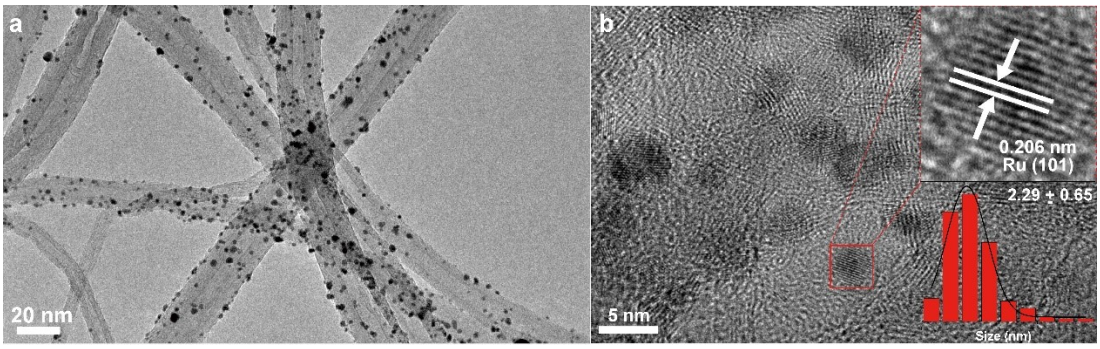

Fig. S4. The low-magnification TEM (a) and (b) HRTEM image of Ru/mCNTs.

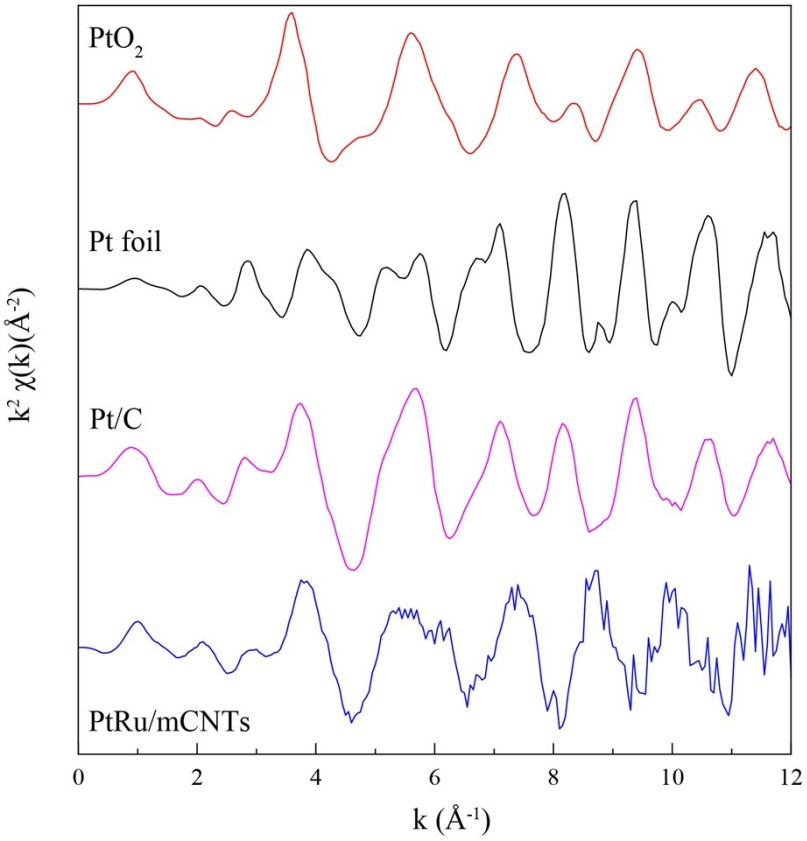

Fig. S5. $k^2\chi$(k) oscillations of Pt L_3-edge EXAFS analysis for the PtRu/mCNTs and references.

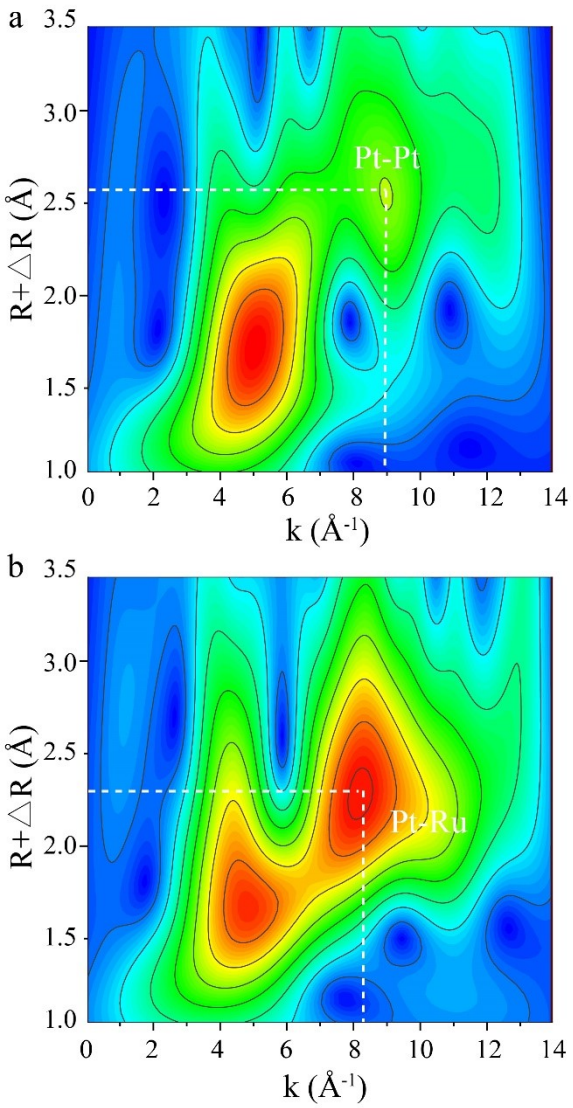

Fig. S6. Wavelet transforms for commercial Pt/C (a) and PtRu/mCNTs (b).

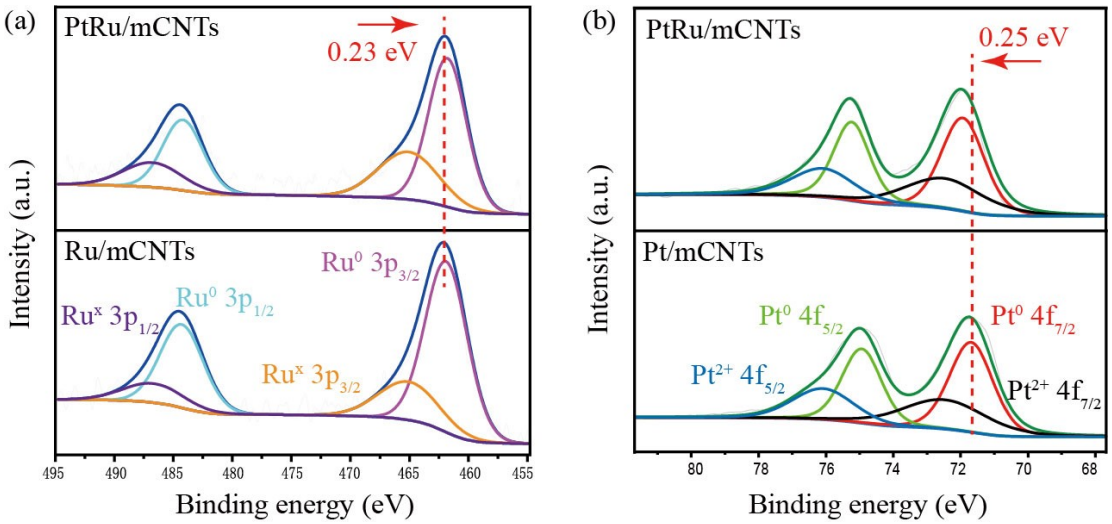

Fig. S7. XPS patterns of Pt/mCNTs, Ru/mCNTs, and PtRu/mCNTs, in Ru 3p (a) and Pt 4f (b) regions.

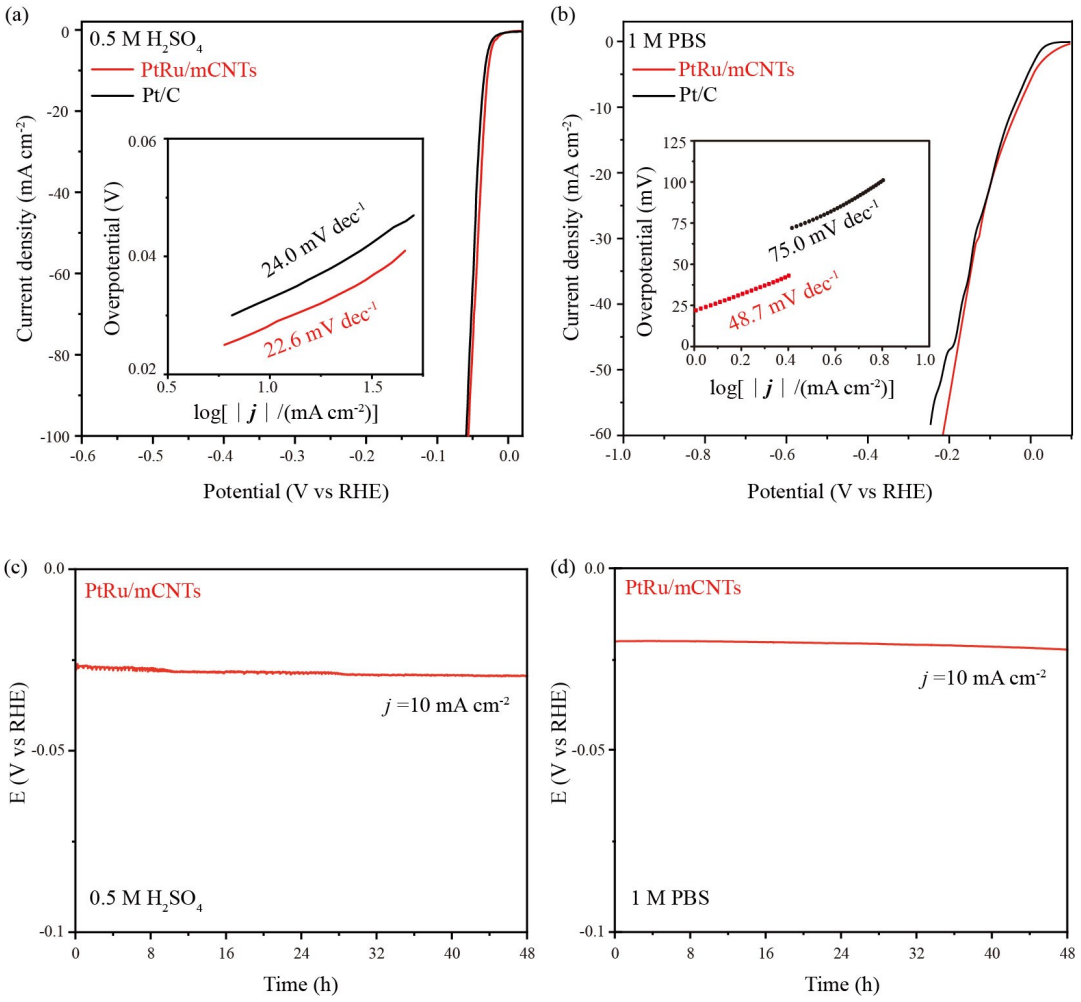

Fig. S8. HER polarization curves and Tafel plots for the PtRu/mCNTs and commercial Pt/C in (a) 0.5 M H_2SO_4 and (b) 1 M PBS. Chronopotentiometry tests of PtRu/mCNTs at a constant current density of 10 mA cm^{-2} in (c) 0.5 M H_2SO_4 and (d) 1 M PBS.

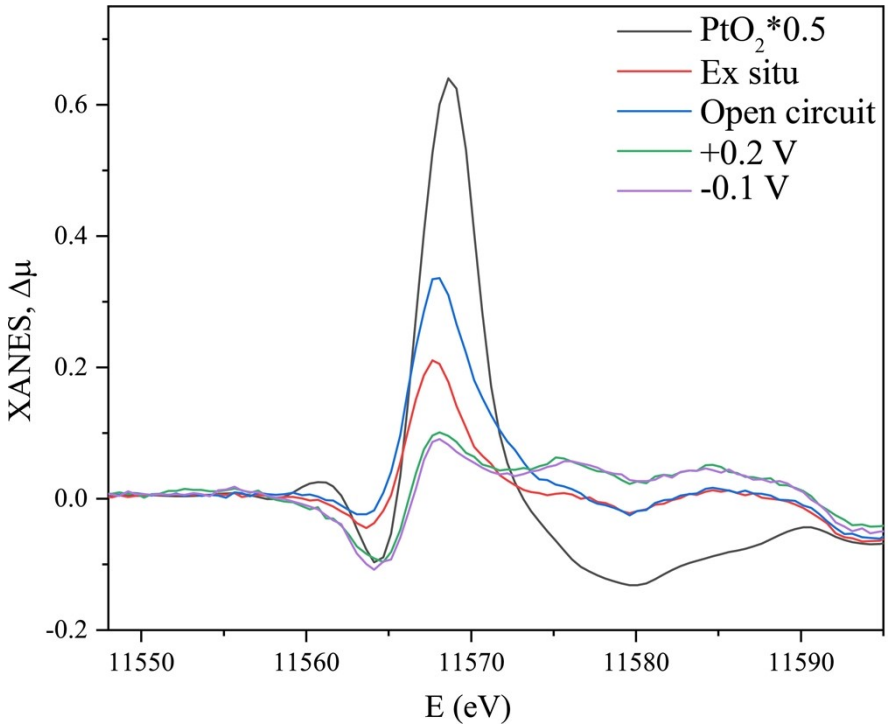

Fig. S9. Normalized difference spectra for Pt L_3-edge XANES using Pt foil as reference.

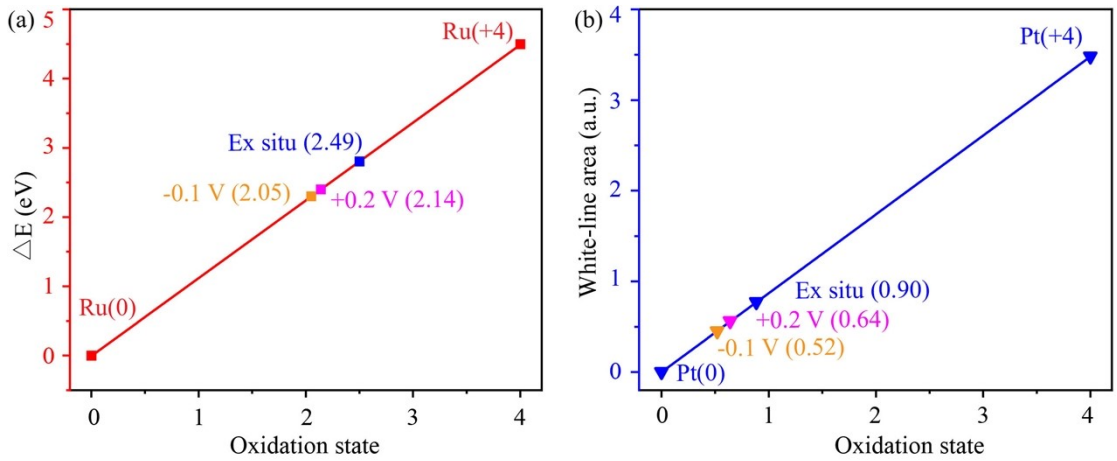

Fig. S10. The fitted average oxidation states of Pt and Ru from XANES spectra.

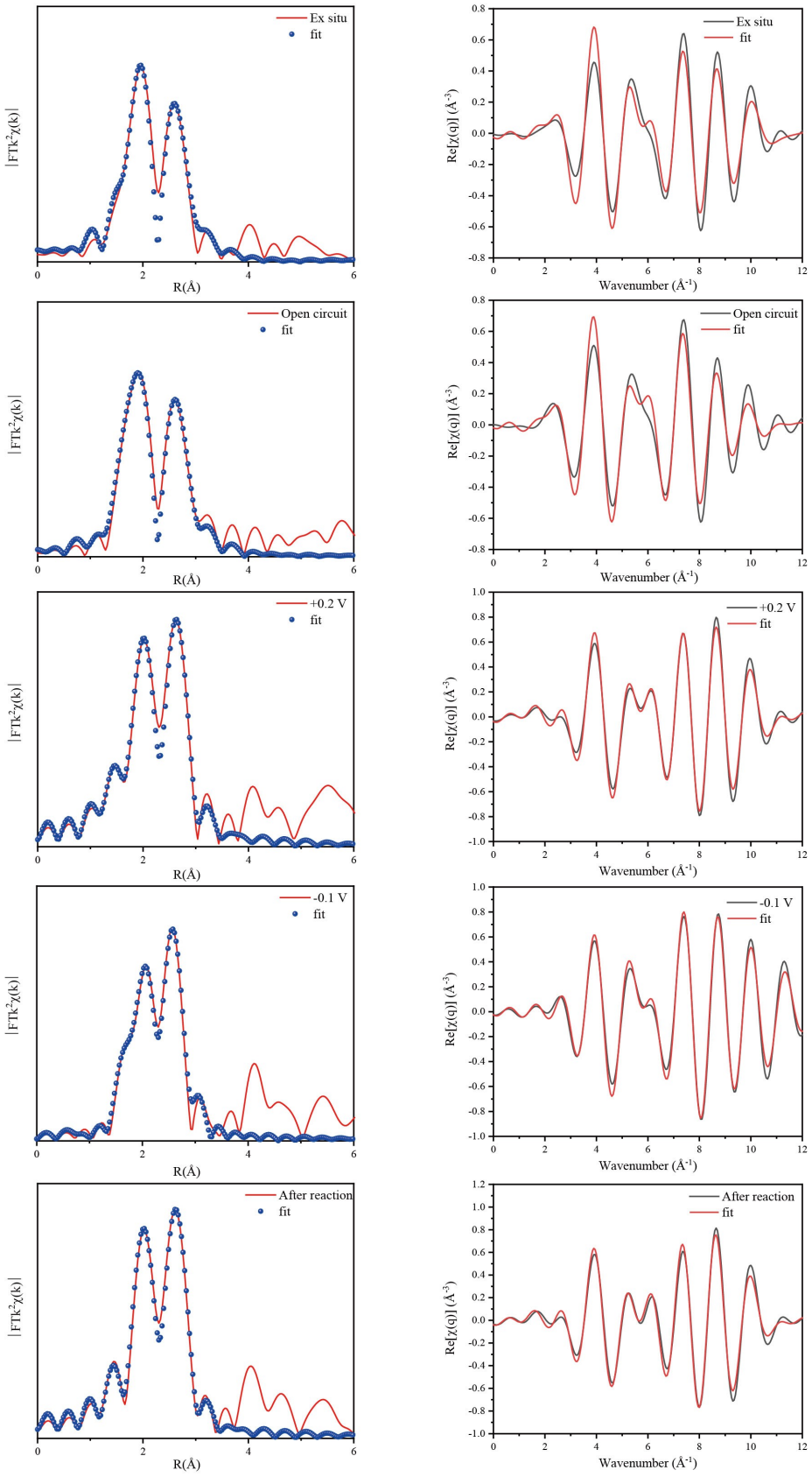

Fig. S11. Least-squares curve-fitting analysis of operando EXAFS spectra at the Pt L_3-edge and corresponding Re($k^2\chi$(k)) oscillations.

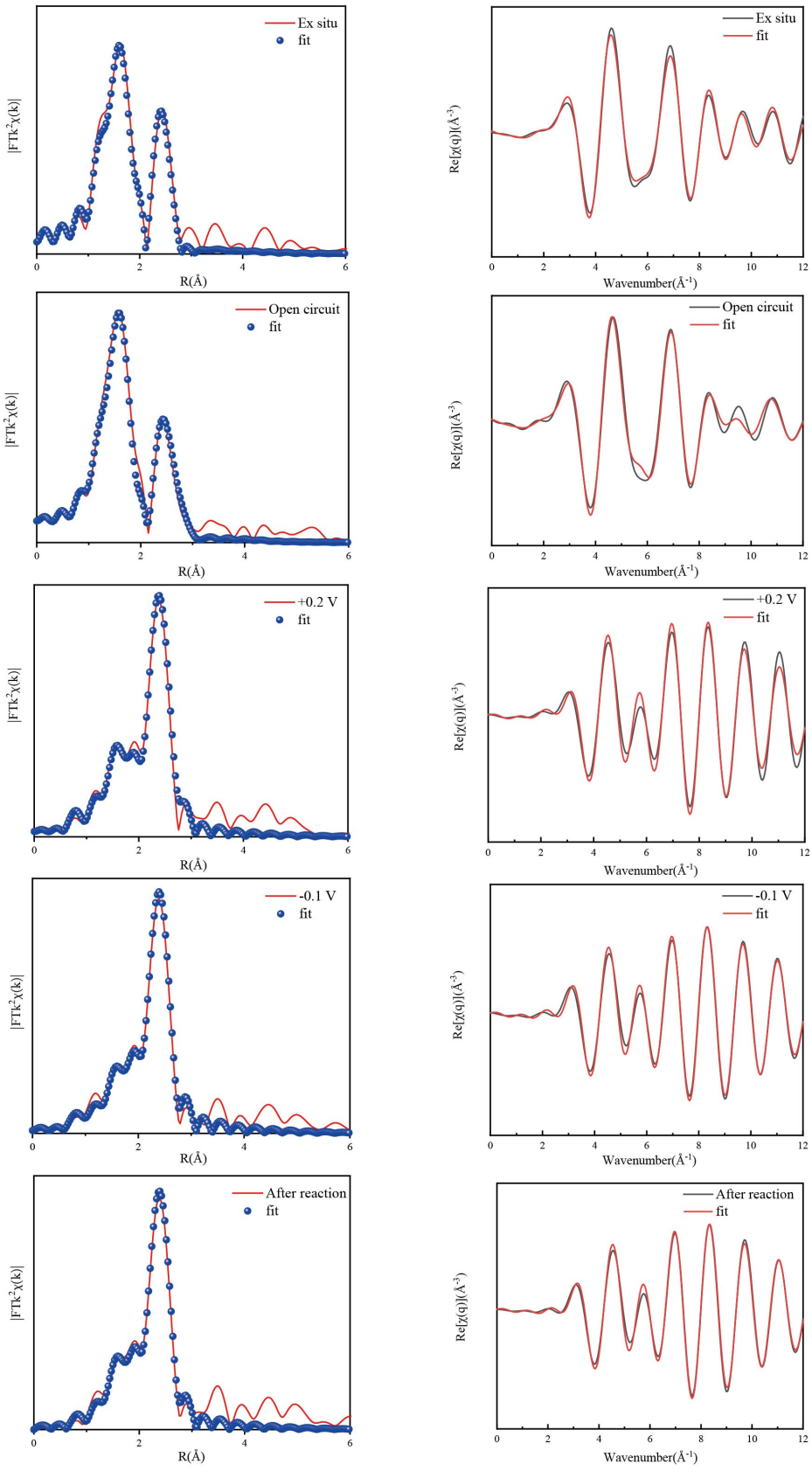

Fig. S12. Least-squares curve-fitting analysis of operando EXAFS spectra at the Ru K-edge and corresponding Re($k^2\chi$(k)) oscillations.

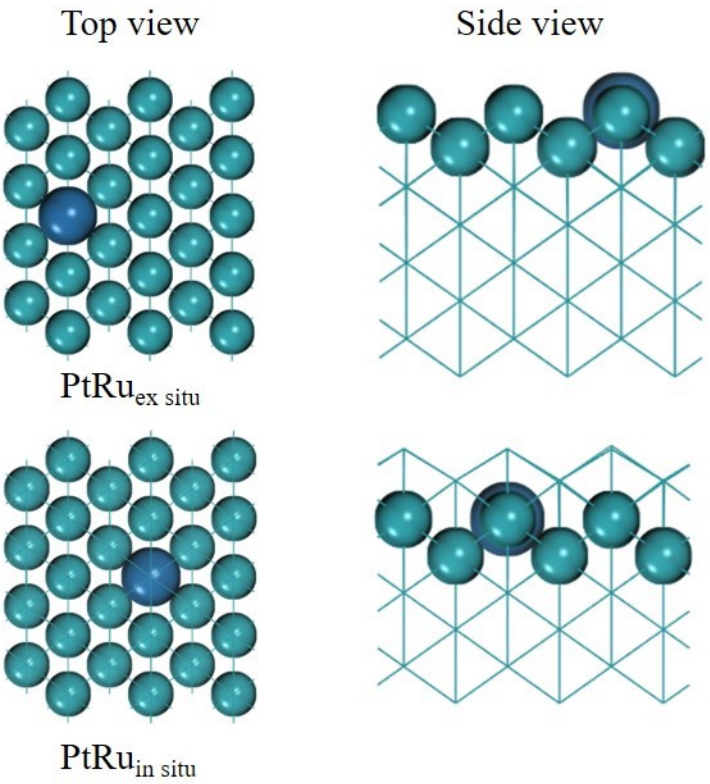

Fig. S13. Atomic model of $PtRu_{ex\ situ}$ and $PtRu_{in\ situ}$ (110) surface, blue ball represents Pt atom and green indicate Ru atom.

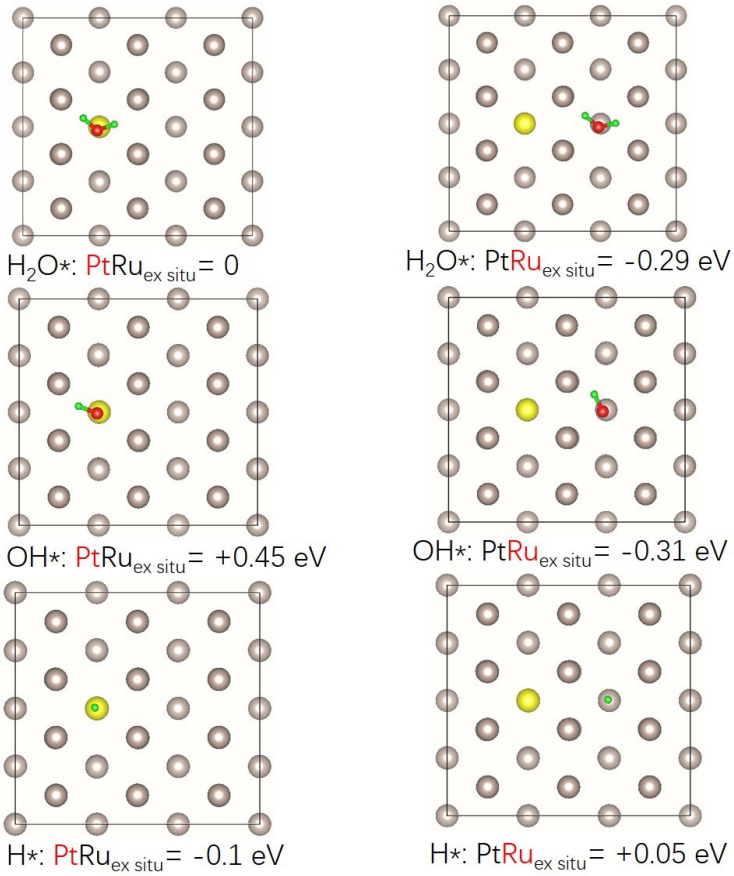

Fig. S14. The adsorption energies of H_2O, OH* and H* models on different metal active sites of $PtRu_{ex\ situ}$.

The adsorption energy of adsorbents (H_2O*, OH* and H*) on $PtRu_{ex\ situ}$ was calculated by: $\Delta G_{ad}=G_{tot} - G_{PtRu}-G_X$. Where G_{tot}, $G_{Pt\text{-}Ru}$, and G_x are the DFT energy of species absorbed on $PtRu_{ex\ situ}$, adsorbate-free $PtRu_{ex\ situ}$, and adsorbed species, respectively.

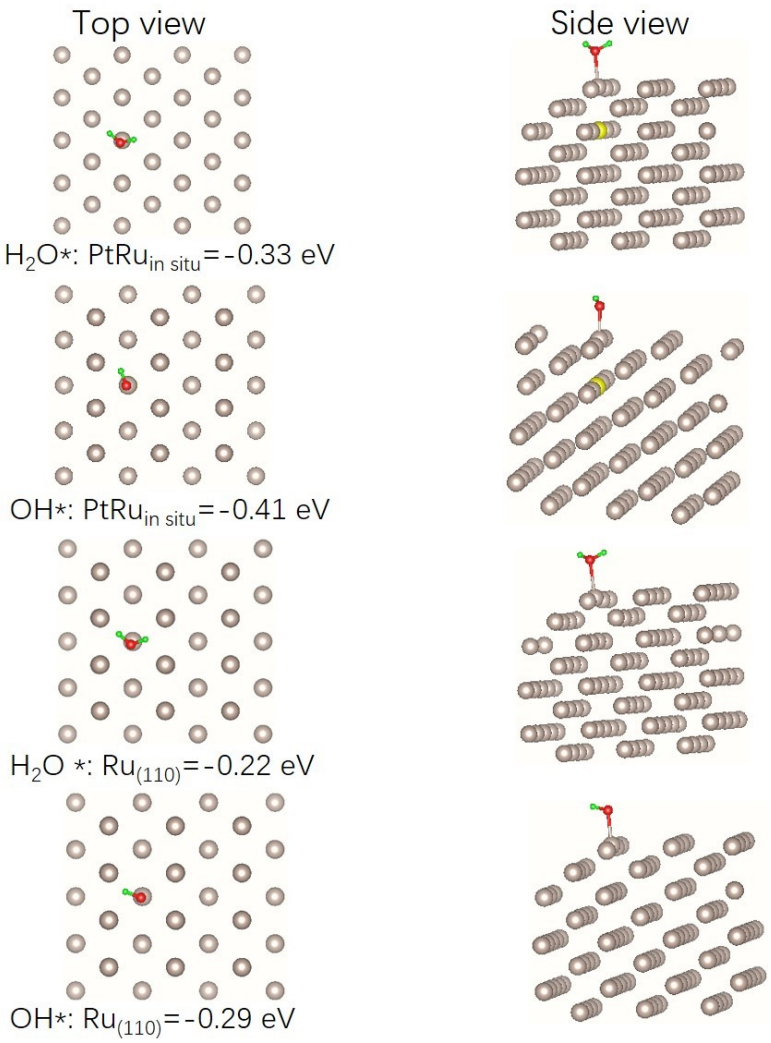

Fig. S15. The adsorption energies of H_2O and OH* models on $PtRu_{in\ situ}$ and Ru (110).

The adsorption energy of adsorbents (H_2O* and OH*) on $PtRu_{in\ situ}$ was calculated by: $\Delta G_{ad}=G_{tot} - G_{PtRu}-G_X$. Where G_{tot}, $G_{Pt\text{-}Ru}$, and G_x are the DFT energy of species absorbed on $PtRu_{in\ situ}$, adsorbate-free $PtRu_{in\ situ}$, and adsorbed species, respectively.

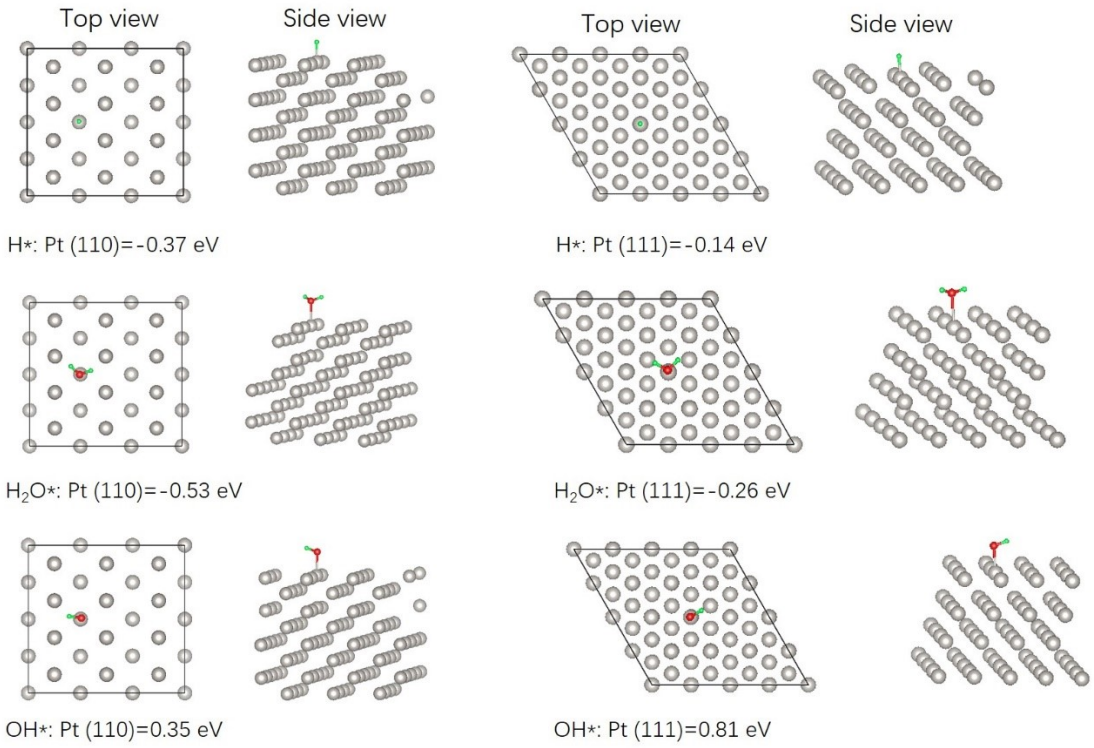

Fig. S16. The adsorption energies of H*, H_2O, and OH* models on Pt (110) and Pt (111).

The adsorption energy of adsorbents (H*, H_2O*, and OH*) on Pt (110) was calculated by: $\Delta G_{ad}=G_{tot}-G_{Pt}-G_X$. Where G_{tot}, G_{Pt}, and G_x are the DFT energy of species absorbed on Pt (110), adsorbate-free Pt (110), and adsorbed species, respectively. The adsorption energy of adsorbents (H*, H_2O*, and OH*) on Pt (111) was calculated by: $\Delta G_{ad}=G_{tot}-G_{Pt}-G_X$. Where G_{tot}, G_{Pt}, and G_x are the DFT energy of species absorbed on Pt (111), adsorbate-free Pt (111), and adsorbed species, respectively.

Table S1. The ICP-AES results of Pt/mCNTs, Ru/mCNTs, and PtRu/mCNTs samples.

Catalysts / Content	Pt (wt%)	Ru (wt%)	Pt (at%)	Ru (at%)
Pt/mCNTs	**0.57**	/	/	/
Ru/mCNTs	/	**5.51**	/	/
PtRu/mCNTs	**0.57**	**5.78**	**5%**	**95%**

Table S2. Summary of some recently reported representative HER electrocatalysts in alkaline electrolytes.

Catalyst	Current density (mA cm^{-2})	Overpotential (mV)	Tafel slope (mV $decade^{-1}$)	References
PtRu/mCNTs	10	15	33.5	**This work**
Ru-MnFeP/NF	10	35	36	7
PtCo-Co/TiM	10	28	35	8
Pt_{SA}-$Co(OH)_2$@Ag	10	29	35.72	9
2DPC-RuMo	10	18	25	10
$CoRu_{0.5}$/CQDs	10	18	38.5	11
Rh-Doped CoFe-LDH	10	28	42.8	12
DSIrNi @CNTS	10	17	48	13
Ru@GnP	10	22	28	14
RuAu-0.2	10	24	37	15
Ru-NPs/SAs@N-TC	10	97	58	16

Table S3. Summary of some recently reported representative HER electrocatalysts in acidic electrolytes.

Catalyst	Current density (mA cm^{-2})	Overpotential (mV)	Tafel slope (mV $decade^{-1}$)	References
PtRu/mCNTs	10	28	22.6	**This work**
Ru/GLC	10	35	30	17
Pt-VGNSAs/CC	10	28.5	60	18
Pt/f-MWCNTs	10	43.9	30	19
Pt-rEGO	10	28.27	32.5	20
RuNi/CQDs	10	58	55	21
Pt/$RuCeO_x$-PA	10	41	31	22
ECM@Ru	10	63	47	23
MXene@Pt/SWCNTs	10	62	78	24
Ru NPs	10	96	78	25
Pt/def-WO_3@CFC	10	42	101.8	26

Table S4. Summary of some recently reported representative HER electrocatalysts in neutral electrolytes.

Catalyst	Current density (mA cm^{-2})	Overpotential (mV)	Tafel slope (mV $decade^{-1}$)	References
PtRu/mCNTs	10	17	48.7	**This work**
Pt-Pd@NPA	10	34.8	32.2	27
Rh_2P	10	38	46	28
Mo_2C@NC@Pt	10	25	33	29
Pt/np-$Co_{0.85}Se$	10	55	35	30
PtRu	10	25	36	31
RuNi/CQDs	10	18	76	21
Rh_2S_3/NC	10	46	37	32
RuCo@NC-600	10	60	38	33

Table S5. Structural parameters of PtRu alloy at the Pt L_3-edge extracted from quantitative EXAFS curve-fittings using the ARTEMIS module of IFEFFIT.

Sample	Path	CN	R(Å)	$\sigma^2(10^{-3}Å^2)$	ΔE_0 (eV)
Pt foil	Pt-Pt	12	2.77		
Pt/C	Pt-Pt	9.2	2.74		
Ex situ	Pt-Cl	1.7	2.29	11.2	9.7
	Pt-Ru	6.7	2.71	14.2	5.2
Open circuit	Pt-Cl	1.7	2.26	11.2	8.5
	Pt-Ru	6.7	2.71	14.2	5.2
+0.2 V	Pt-Cl	1.0	2.35	8.3	9.5
	Pt-Ru	7.9	2.71	11.8	5.1
-0.1 V	Pt-Cl	1.1	2.37	7.1	9.8
	Pt-Ru	9.1	2.68	13.5	2.3
After reaction	Pt-Cl	0.9	2.36	7.9	9.8
	Pt-Ru	8.1	2.71	12.0	5.0

CNs, coordination numbers; R, bonding distance; σ^2, Debye-Waller factor; ΔE_0, inner potential shift.

Table S6. Structural parameters of PtRu alloy at the Ru K-edge extracted from quantitative EXAFS curve-fittings using the ARTEMIS module of IFEFFIT.

Sample	Path	CN	R(Å)	$\sigma^2(10^3Å^2)$	ΔE_0 (eV)
Ru foil	Ru-Ru	12	2.65		
Ex situ	Ru-O	3.5	2.00	5.2	1.7
	Ru-Ru	8.5.	2.65	15.4	-0.3
	Ru-Pt	0.7	2.71	7.7	9.5
Open circuit	Ru-O	3.9	2.00	6.2	3.8
	Ru-Ru	8.5	2.65	14.4	-2.1
	Ru-Pt	0.9	2.71	8.5	9.5
+0.2 V	Ru-O	2.1	2.02	7.0	1.6
	Ru-Ru	8.5	2.66	10.1	-1.4
	Ru-Pt	1.3	2.70	9.3	9.5
-0.1 V	Ru-O	1.4	2.02	6.5	1.6
	Ru-Ru	8.5	2.66	9.0	-1.0
	Ru-Pt	1.5	2.68	10.2	9.4
After reaction	Ru-O	1.9	2.02	6.6	3.9
	Ru-Ru	8.5	2.66	10.7	-1.1
	Ru-Pt	1.5	2.70	10.1	9.2

CNs, coordination numbers; R, bonding distance; σ^2, Debye-Waller factor; ΔE_0, inner potential shift.

References:

1. J. Hafner, *J. Comput. Chem.*, 2008, **29**, 2044-2078.
2. P. E. Blochl, *Phys. Rev. B. Condens. Matter.*, 1994, **50**, 17953-17979.
3. G. J. Kresse, D., *Phys. Rev. B.*, 1999, **59**, 1758-1775.
4. K. B. John P. Perdew, Matthias Ernzerhof, *Phys. Rev. Lett.*, 1996, **77**, 3865-3868.
5. S. Grimme, *J Comput Chem*, 2006, **27**, 1787-1799.
6. K. Mathew, R. Sundararaman, K. Letchworth-Weaver, T. A. Arias and R. G. Hennig, *J. Chem. Phys.*, 2014, **140**, 084106.
7. D. Chen, Z. Pu, R. Lu, P. Ji, P. Wang, J. Zhu, C. Lin, H. W. Li, X. Zhou, Z. Hu, F. Xia, J. Wu and S. Mu, *Adv. Energy. Mater.*, 2020, **10**, 2000814.
8. Z. Wang, X. Ren, Y. Luo, L. Wang, G. Cui, F. Xie, H. Wang, Y. Xie and X. Sun, *Nanoscale.*, 2018, **10**, 12302-12307.
9. K. L. Zhou, C. Wang, Z. Wang, C. B. Han, Q. Zhang, X. Ke, J. Liu and H. Wang, *Energ. Environ. Sci.*, 2020, **13**, 3082-309.
10. K. Tu, D. Tranca, F. Rodríguez-Hernández, K. Jiang, S. Huang, Q. Zheng, M. X. Chen, C. Lu, Y. Su, Z. Chen, H. Mao, C. Yang, J. Jiang, H. W. Liang and X. Zhuang, *Adv. Mater.*, 2020, **32**, 2005433.
11. W. Li, Y. Zhao, Y. Liu, M. Sun, G. I. N. Waterhouse, B. Huang, K. Zhang, T. Zhang and S. Lu, *Angew. Chem. Int. Edit.*, 2020, **133**, 3327-3335.
12. K. Zhu, J. Chen, W. Wang, J. Liao, J. Dong, M. O. L. Chee, N. Wang, P. Dong, P. M. Ajayan, S. Gao, J. Shen and M. Ye, *Adv. Funct. Mater.*, 2020, **30**, 2003556.
13. S. Liu, Z. Hu, Y. Wu, J. Zhang, Y. Zhang, B. Cui, C. Liu, S. Hu, N. Zhao, X. Han, A. Cao, Y. Chen, Y. Deng and W. Hu, *Adv. Mater.*, 2020, **32**, 2006034.
14. F. Li, G. F. Han, H. J. Noh, I. Ahmad, I. Y. Jeon and J. B. Baek, *Adv. Mater.*, 2018, **30**, 1803676.
15. C. H. Chen, D. Wu, Z. Li, R. Zhang, C. G. Kuai, X. R. Zhao, C. K. Dong, S. Z. Qiao, H. Liu and X. W. Du, *Adv. Energy. Mater.*, 2019, **9**, 1803913.
16. B. Yan, D. Liu, X. Feng, M. Shao and Y. Zhang, *Adv. Funct. Mater.* 2020, **30**, 2003007.
17. Z. Chen, J. Lu, Y. Ai, Y. Ji, T. Adschiri and L. Wan, *ACS. Appl. Mater. Inter.*, 2016, **8**, 35132-35137.
18. H. Zhang, W. Ren, C. Guan and C. Cheng, *J. Mater. Chem. A*, 2017, **5**, 22004-22011.
19. J. Ji, Y. Zhang, L. Tang, C. Liu, X. Gao, M. Sun, J. Zheng, M. Ling, C. Liang and Z. Lin, *Nano. Energy.*, 2019, **63**, 103849.
20. Y. Peng, J. Cao, J. Yang, W. Yang, C. Zhang, X. Li, R. A. W. Dryfe, L. Li, I. A. Kinloch and Z. Liu, *Adv. Funct. Mater.*, 2020, **30**, 2001756.
21. Y. Liu, X. Li, Q. Zhang, W. Li, Y. Xie, H. Liu, L. Shang, Z. Liu, Z. Chen, L. Gu, Z. Tang, T. Zhang and S. Lu, *Angew. Chem. Int. Edit.*, 2020, **59**, 1718-1726.
22. W. G. Tongtong Liu, Qiqi Wang, Meiling Dou, Zhengping Zhang, and Feng Wang, *Angew. Chem. Int. Edit.*, 2020, **59**, 20423-20427.
23. H. Zhang, W. Zhou, X. F. Lu, T. Chen and X. W. Lou, *Adv. Energy. Mater.*,

2020, **10**, 2000882.
24. C. Cui, R. Cheng, H. Zhang, C. Zhang, Y. Ma, C. Shi, B. Fan, H. Wang and X. Wang, *Adv. Funct. Mater.*, 2020, **30**, 2000693.
25. S. G. Patra, K. Sathiyan, M. Meistelman and T. Zidki, *Isr. J. Chem.*, 2020, **60**, 630-637.
26. H. Tian, X. Cui, L. Zeng, L. Su, Y. Song and J. Shi, *J. Mater. Chem. A.*, 2019, **7**, 6285-6293.
27. C. Yang, H. Lei, W. Z. Zhou, J. R. Zeng, Q. B. Zhang, Y. X. Hua and C. Y. Xu, *J. Mater. Chem. A.*, 2018, **6**, 14281-14290.
28. F. Yang, Y. Zhao, Y. Du, Y. Chen, G. Cheng, S. Chen and W. Luo, *Adv. Energy. Mater.*, 2018, **8**, 1703489.
29. J. Q. Chi, J. Y. Xie, W. W. Zhang, B. Dong, J. F. Qin, X. Y. Zhang, J. H. Lin, Y. M. Chai and C. G. Liu, *ACS. Appl. Mater. Inter.*, 2019, **11**, 4047-4056.
30. K. Jiang, B. Liu, M. Luo, S. Ning, M. Peng, Y. Zhao, Y. R. Lu, T. S. Chan, F. M. F. de Groot and Y. Tan, *Nat. Commun.*, 2019, **10**, 1743.
31. L. Li, G. Zhang, B. Wang, T. Yang and S. Yang, *J. Mater. Chem. A.*, 2020, **8**, 2090-2098.
32. C. Zhang, H. Liu, Y. Liu, X. Liu, Y. Mi, R. Guo, J. Sun, H. Bao, J. He, Y. Qiu, J. Ren, X. Yang, J. Luo and G. Hu, *Small. Methods.*, 2020, **4**, 2000208.
33. F. Zhang, Y. Zhu, Y. Chen, Y. Lu, Q. Lin, L. Zhang, S. Tao, X. Zhang and H. Wang, *J. Mater. Chem. A.*, 2020, **8**, 12810-12820.